Vibrational and electronic properties of 4 '-halomethyl-2-biphenylcarbonitrile compounds

Rao, Y. B. Shankar

2017-09-15

Rao , Y B S , Veeraiah , V , Sundius , T & Chaitanya , K 2017 , ' Vibrational and electronic properties of 4 '-halomethyl-2-biphenylcarbonitrile compounds ' , Journal of Molecular Structure , vol. 1144 , pp. 313-323 . https://doi.org/10.1016/j.molstruc.2017.05.053

http://hdl.handle.net/10138/234780
https://doi.org/10.1016/j.molstruc.2017.05.053

Accepted Manuscript

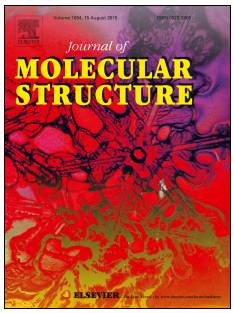

Vibrational and electronic properties of 4′-halomethyl-2-biphenylcarbonitrile compounds

Y.B. Shankar Rao, V. Veeraiah, Tom Sundius, Kadali Chaitanya

PII: S0022-2860(17)30637-3

DOI: 10.1016/j.molstruc.2017.05.053

Reference: MOLSTR 23794

To appear in: *Journal of Molecular Structure*

Received Date: 1 November 2016

Revised Date: 26 April 2017

Accepted Date: 12 May 2017

Please cite this article as: Y.B. Shankar Rao, V. Veeraiah, T. Sundius, K. Chaitanya, Vibrational and electronic properties of 4′-halomethyl-2-biphenylcarbonitrile compounds, *Journal of Molecular Structure* (2017), doi: 10.1016/j.molstruc.2017.05.053.

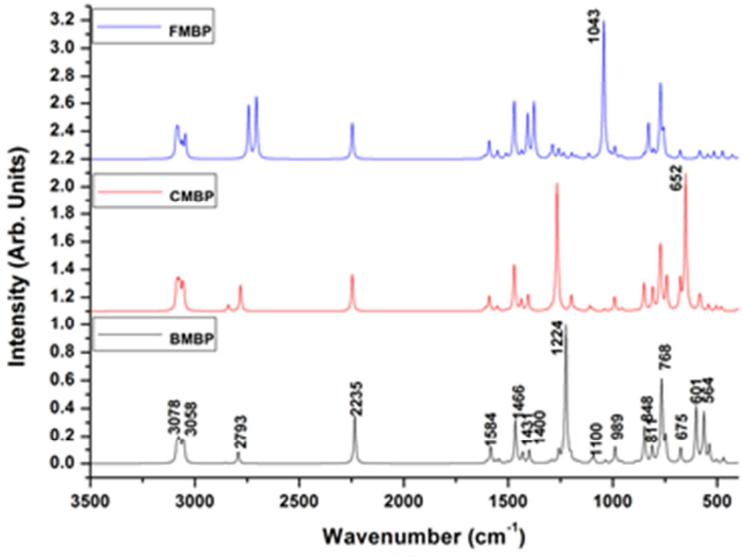

Vibrational and electronic properties of 4′-halomethyl-2-biphenylcarbonitrile compounds

Y.B. Shankar Rao[a, b], V. Veeraiah[a], Tom Sundius[c], Kadali Chaitanya[d,1]

[a] Department of Physics, Andhra University, Visakhapatnam, India
[b] Department of Physics, Anil Neerukonda Institute of Technology & Sciences, Bheemunipatnam, Visakhapatnam, India
[c] Department of Physics, University of Helsinki, Helsinki, Finland
[d] Department of Chemistry, Nanjing University of Science and Technology, Nanjing, China

Abstract

In this paper we studied the structural, vibrational and electronic properties of the 4′-bromomethyl-2-biphenylcarbonitrile (BMBP) 4′-chloromethyl-2-biphenylcarbonitrile (CMBP) and 4′-fluoromethyl-2-biphenylcarbonitrile (FMBP) compounds using experimental and theoretical methods. The FT-IR and FT-Raman spectra of BMBP in solid phase were recorded in the region 4000–400 cm^{-1} and 4000–50 cm^{-1}, respectively. The UV absorption spectrum of BMBP was recorded in dichloromethane and methanol solvents in the range 180–400 nm. The theoretical spectral properties of title compounds were simulated using density functional theory (DFT) and time dependent DFT methods. Scaling of the vibrational frequencies was carried out with the MOLVIB program using multiple scaling factors and assignment to each vibrational frequency was consigned on the basis of potential energy distribution (PED). The electronic spectrum of BMBP in two different solvents (methanol and dichloromethane), calculated at the CAM-B3LYP/6-31G(d,p) level compares well with the experimental data and validates the current method for predicting the absorption spectrum of CMBP and FMBP. Furthermore, the electronic, nonlinear optical and thermodynamics properties of the three compounds were discussed in detailed.

Keywords: vibrational spectra, electronic spectra, DFT, TDDFT, Molvib

[1] Corresponding author E-mail : cskcmail@gmail.com

1. Introduction

Biphenyl derivatives are used as intermediates in the synthesis of heterocyclic compounds for biological applications [1-3]. Murugesan et al recommend that a structure-activity relationship of dual receptor antagonists is better through the manifestation of a biphenyl group [4]. Generally, the biological properties of biphenyls vary considerably and are remarkably dependent on the pivot bond and position of the substituent. Besides, the substituent site plays a prevailing character in determining the phenyl-ring twist angle, which is directly correlated with the biological activity of the biphenyl [5]. In 1981, Mckinney and Singh explored the structure-activity relationships in halogenated biphenyls and concluded that of the biphenyl systems only the coplanar or nearly coplanar conformers are active in binding the receptor for cytochrome P-448 induction [6].

On the other hand, vibrational and electronic spectroscopies were proven to be great techniques for interpreting structural and electronic properties of biological molecules. Normally, the presence of a substituent group in phenyl rings leads to the difference of charge distribution in molecules, and thus this significantly affects the structural, electronic and vibrational parameters. Vibrational spectra, measured through IR and Raman techniques, on biphenyl/substituted biphenyls have been reported by some researchers in different phases such as liquid and crystals [7–13]. The complete fundamental frequencies and molecular configuration of biphenyl has been reported elsewhere in literature [13]. The vibrational spectra of biphenyl in the ground and first excited triplet state been investigated by using quantum chemical calculations by Lee [11]. The spectral studies on the vibrational frequencies of 4,4'-d_2-biphenyl and 4,4'-dihalogenated biphenyls were reported by a few authors [8-10]. Many experimental and theoretical electronic absorption spectra of biphenyl and its derivatives have been published [14-25]. The biphenyl shows a structureless intense band at 247 nm in a non-polar solvent. This band shifted to higher/lower wavelengths upon inclusion of a substituent group in phenyl rings. In 1964, Gondo has calculated the electronic transition energies of biphenyl, in which the effects of twisting the pivot bond in biphenyl are taken into account [22]. Berlman and Steingraber have determined the fluorescence lifetime of biphenyl and found a hidden band on the longer-wavelength side of the intense 247 nm band [26]. Recently, several researchers investigated the vibrational properties of 4-methyl-2-cyanobiphenyl using both experimental and theoretical studies and gave the final assignment on the basis of normal coordinate treatment [17, 27, 28].

Apart from above discussion, the detailed calculations coupled with experimental work on biphenyl or mono-/di-substituted biphenyls, there have so far been no other

significant studies reported. Therefore, in this study we have chosen 4′-halomethyl-2-biphenylcarbonitrile (halo = bromine, chlorine and fluorine) compounds, among which only 4′-bromomethyl-2-biphenylcarbonitrile is synthetically accessible and well known as a key intermediate in the production of Losartan and is very useful in the treatment of hypertension by inhibiting angiotensin II [29]. The crystal structure of this compound is reported by Song et al in 2003 [30]. Unfortunately due to the unavailability of chlorine and fluorine derivatives of methyl-2-biphenylcarbonitrile, in this work we mainly focused on interpreting complete spectral assignments of experimentally obtained vibrational and electronic spectra of 4′-bromomethyl-2-biphenylcarbonitrile (BMBP). Furthermore, to understand the influence of halogen substituent on the spectral characteristics, the vibrational and electronic properties of 4′-chloromethyl-2-biphenylcarbonitrile (CMBP) and 4′-fluoromethyl-2-biphenylcarbonitrile (FMBP) compounds were obtained with quantum chemical calculations and compared with the BMBP. Herein, the investigated results have been reported. The results obtained in this studied are valuable for providing a reliable insight into the vibrational and electronic properties of similar compounds.

2. Experimental details

The 4′-bromomethyl-2-biphenylcarbonitrile, BMBP (98% purity) is purchased from TCI chemicals. The FT-IR and FT-Raman spectra of BMBP were recorded with a Nicolet 6700 FT-IR spectrometer with a NXR FT-Raman module. FT-IR spectrum was recorded on samples dispersed in KBr pellets in the range of 400 – 4000 cm^{-1}. The FT-Raman spectrum was recorded on solid samples contained in standard NMR diameter tubes or on compressed samples contained in a gold-coated sample holder. The UV-Visible absorption spectrum of BMBP in dichloromethane and methanol solvents were recorded in the range 200–400 nm using Analytic Jena SPECORD 50PLUS, UV–Vis recording spectrometer.

The experimental setup used in the present investigation of Second Harmonic Generation (SHG) efficiency was similar to the generic one devised by Kurtz, DCR-11-type Nd:YAG laser with a pulse energy of 3 mJ/pulse was used as a source. A microcrystalline powdered sample of BMBP was tightly packed in a glass capillary and exposed to a fundamental wave with a pulse width of 8 ns, repetition frequency 10 Hz, and a wavelength of 1064 nm. The generated second harmonic wave of 532 nm was detected by a photomultiplier tube (Hamamatsu-R 2059) and converted into an electrical signal. The electrical signal was displayed on the oscilloscope (Tektronix-TDS 3000B). The signal amplitudes in volts indicate the SHG efficiency of the sample.

Figure 1

3. Computational details

All the calculations in this study were carried out using Gaussian 03W program [31]. The initial structure of the three compounds is taken from the available crystal structure data of BMBP[30] and then optimized using B3LYP / 6-31G(d,p) level of theory [32]. This method is most widely adopted for calculating vibrational frequencies of organic molecules.

Generally, the calculated vibrational frequencies are larger than the experimental frequencies due to the anharmonic effects, combination of electron correlation effects and the basis set deficiencies. Therefore, we have scaled down the vibrational frequencies using a scaled quantum mechanical (SQM) procedure [33-34]. The normal coordinate analysis with potential energy distribution (PED) was done with the MOLVIB program written by Sundius [35]. The UV–Vis absorption spectra, electronic transitions, vertical excitation energies, absorbance and oscillator strength were computed with the TD- approach using the CAM-B3LYP functional. Other quantum chemical parameters and nonlinear optical properties of the title compounds were calculated at the B3LYP / 6-31G(d,p) level of theory.

4. Results and Discussion

4.1. Molecular Geometry

Table 1

Initial structure of the title molecules was generated from the available crystal structure data of BMBP [30]. The optimized structure parameters of BMBP, CMBP and FMBP were calculated at the DFT/B3LYP level with the 6-31G(d,p) basis set along with the experimental data of BMBP [30] in Table 1 in accordance with the atom numbering scheme given in Fig. 1. From Table 1 we can notice that the calculated bond lengths and bond angles of BMBP are in good agreement with the experimental data. The maximum difference between experimental and calculated bond lengths and bond angles is 0.046 and 1.684, respectively. This means that the structural parameters obtained for CMBP and FMBP with the current method are consistent and adequate. When compared to the un-substituted biphenyl, the cyano and bromomethyl substituents on the phenyl rings have significant effect on the ring twist (from the visual inspection with GaussView, the dihedral angle between the two phenyl rings C_2-C_1-C_7-C_{12} of the BMBP compound is found to be 48.23°), and the value is analogous with the experimental value of 48.34° found for the orthorhombic form of 4'-bromomethylbiphenyl-2-carbonitrile [30]. However, in the case of CMBP and FMBP the

dihedral angle between two phenyl rings were found to be 47.55° and 46.92° , which shows that the twist angle decreases with increasing electronegativity of the halogen group. This significant twist angle is attributable to the flipping of the ring containing halomethyl with respect to twofold rotation axis located at the midpoint of the biphenyl C_1-C_7 bond is caused by the decrease in the pivot C_1-C_7 bond length and increase in steric interactions between the ortho hydrogens. From Table 1 we can also observe that the C-X (X = Br, Cl and F) bond lengths decrease with increasing electronegativity of the halogen atom. Apart from above discussed points there were no appreciable changes in the structural parameters of three compounds when compared to each other.

4.2. Vibrational analysis

The symmetry of the title molecules is considered as C_1 and having 26 atoms each. Therefore, all the 72 normal modes of vibrations are IR and Raman active. The identification of the normal modes of BMBP with the DFT calculation and the analysis of PED contributions allowed us to know the origin of all bands appearing in both the infrared and Raman spectra of the BMBP. In order to obtain the normal modes in a molecular coordinate system, internal coordinates and the local symmetry coordinates for the investigated molecules were presented in Table S1 and Table S2. The RMS deviation of the observed and calculated frequencies (unscaled) of BMBP was found to be 59.1 cm^{-1}, respectively. In order to mimic the observed frequencies, the scale factors were refined and optimized via a least squares refinement algorithm which resulted into a weighed RMS deviation of 3.67 cm^{-1} between the experimental and scaled quantum mechanical (SQM) frequencies. This indicates that the theoretical IR and Raman spectra of BMBP agreed well with the experimental FT-IR and FT-Raman spectra and endorses the present method for computing the IR and Raman spectra of CMBP and FMBP. For full understanding we have presented the observed and simulated FT-IR and FT-Raman spectra of BMBP in Fig. 2 and simulated IR and Raman spectra of three molecules in Fig. 3. The full details of vibrational assignments attempted in Table 2 are given below.

Table 2

Figure 2

C-H group vibrations

The C–H stretching vibrations in the biphenyl belong to the a_1 (3086, 3052, 3038 cm^{-1}) and b_2 (3086, 3038 cm^{-1}) species [7]. Generally, in the C–H stretching region, the bands are not appreciably affected by the substituents. For BMBP, the FT-IR bands at 3056, 3028

cm^{-1} and FT-Raman bands at 3088, 3060, 3039 cm^{-1} have been assigned to the C–H stretching vibrations. In general most of them are weak in either the FT-Raman or FTIR, with the exception of 3060 cm^{-1} , which appears as very strong band in the FT-Raman spectra and is assigned to the C–H in-phase stretching mode of ring B. Numerous studies show that a small change in structure of the molecule lead to significant changes in its vibrational spectra. For example, varying the substituents on the molecule shifts certain bands in the vibrational spectra to higher or lower wavenumbers with a large change in their intensity. However, as compared to BMBP, the frequencies pertaining to the C-H stretching vibration in CMBP and FMBP do not show any significant change in IR spectra, but from Raman spectra we have noticed that the band intensities are increasing with increasing electronegativity of the substituent.

The C–H in-plane bending vibrations appear in the region 1000-1520 cm^{-1} [36–38]. The bands corresponding to the C–H in-plane bending modes belonging to the a_1 and b_2 species of biphenyl are observed at 1182, 1012 cm^{-1} and 1250, 1162, 1082 cm^{-1} in the IR spectra [7]. However, in the present study the eight C–H in-plane bending vibrations of BMBP are assigned on the basis of PED analysis. The results indicate that the calculated modes are dominated by C–H in-plane bending, and coupled mostly with CC stretching. Among eight C-H in-plane bending vibrations six were observed and the remaining ones were predicted on the basis of the PED. The bands observed at 1473, 1404, 1324, 1187, 1159, 1133 cm^{-1} and 1481, 1380, 1303, 1188 cm^{-1} in the FT-IR and FT-Raman spectra, respectively are assigned to C–H in-plane bending vibrations. The two C-H in-plane bending vibrations which are not observed both in FT-IR and FT-Raman spectra are predicted at 1504 and 1431 cm^{-1}. However, for CMBP and FMBP, the C-H in-plane bending vibrations are predicted at 1509, 1471, 1438, 1405, 1320, 1183, 1161, 1110 cm-1 and 1510, 1471, 1437, 1407, 1303, 1175, 1161, 1115 cm^{-1}, respectively. The PED analysis shows that these modes mostly have a dominating contribution from C-H in-plane bending (> 60%). From Fig. 3 one can notice that the intensity of the C-H in-plane bending vibrations increases with increasing electronegativity of the halogen substituent.

Figure 3

The C-H out-of-plane vibrations in aromatic compounds are observed mostly in the region 700-1000 cm^{-1} [36-38]. In biphenyl, the C-H out-of-plane vibrations are assigned to the b_1 and a_2 species, which are observed at 969, 904, 738 cm^{-1} and 985, 834 cm^{-1} in the IR spectrum [7]. For the BMBP molecule these vibrations are observed at 953, 882, 833, 758 cm^{-1} in FT-IR spectrum and 825 cm^{-1} in FT-Raman spectrum. All these calculated modes are

in good agreement with the observed values. For CMBP and FMBP, on the basis of PED contributions we have assigned this vibration to the calculated frequencies 987, 962, 960, 954, 889, 850, 843, 771 cm^{-1} and 987, 965, 956, 952, 888, 850, 829, 772 cm^{-1}.

C-C group vibrations

The C–C stretching frequencies of aromatic compounds are largely expected in the region 650-1650 cm^{-1} [36–38]. For instance, in biphenyl the C-C stretching vibrations observed at 1603, 1497 cm^{-1} and 1583, 1448, 1316 cm^{-1} in IR spectrum are assigned to a_1 and b_2 species [38]. However, these modes are affected by substitution in the aromatic ring; with heavy substituents, the bands tend to shift to somewhat lower wavenumbers and the greater the number of substituents on the ring, the broader the absorption regions [38]. In BMBP, the vibrations observed at 1591, 1518, 1268 cm^{-1} in FT-IR and 1597, 1518, 1260, 1049 cm^{-1} in FT-Raman are assigned to C-C stretching vibrations of ring A. However, these vibrations are observed for ring B at 1559, 1134 cm^{-1} and 1614, 1578, 1133, 810 cm^{-1} in the FT-IR and FT-Raman spectra. On the basis of the PED contribution we have predicted this vibration for CMBP (FMBP) at 1608, 1591, 1566, 1551, 1298, 1287, 1260, 1096, 1038, 1011 and 809 cm^{-1} (1612, 1591, 1567, 1522, 1377, 1290, 1287, 1259, 1196, 1096, 1039, 1009 and 805 cm^{-1}). The six C-C-C in-plane and out-of-plane bending vibrations of BMBP are observed in the region 1000 – 500 cm^{-1} and 800 – 380 cm^{-1} and are supported well by the literature data [7]. The frequency observed at 1002 cm^{-1} in FT-IR spectrum of BMBP is assigned to ring breathing modes of ring B. However, for ring A it is predicted at 990 cm^{-1}. The ring symmetric in-plane bending vibration of ring A observed at 684 and 681 cm^{-1} in FT-IR and FT-Raman spectrum. Whereas, this vibration pertaining to ring B is not observed experimentally, but on the basis of the PED contribution this is assigned to calculated frequency 594 cm^{-1}. Weak bands observed at 770 and 642 cm^{-1} in FT-Raman spectra are assigned to the ring in-plane asymmetric deformation of ring A and B. In biphenyl, the ring out-of-plane deformations observed at 696, 470 cm^{-1} and 397 cm^{-1} in IR spectrum are assigned to b_1 and a_2 like species [7]. In the present study, these vibrations are observed at 469, 564, 724 cm^{-1} and 783, 471, 414, 384 cm^{-1} in FT-IR and FT-Raman spectra. All the calculated modes are in good agreement with the observed values. Whereas, for CMBP and FMBP the ring in-plane and out-of-plane vibrations were predicted in the same region (see Table 2).

On the other hand, in the region 1450-1700 cm^{-1}, the vibrational frequencies in IR spectra were not affected by the halogen substituent, as these frequencies belong to the

biphenyl ring C-C stretching and in-plane C-H bending vibrations (see Table 2). However, the C-C stretching vibration (C-H in-plane bending vibration) observed at 1583 cm^{-1} (1503 and 1466 cm^{-1}) in Raman spectra show significant change in bands intensity as going from BMBP to FMBP. The frequency predicted at 1431 cm^{-1} is comparable with the frequency that appeared at 1438 cm^{-1} in both IR and Raman spectra of BMBP, which pertain to C-H in-plane bending vibration, does not sight any substantial change in CMBP and FMBP. In CMBP and FMBP, this vibration is assigned to the predicted values 1438 and 1437 cm^{-1}. Whereas, the band that appeared at 1404 and 1380 cm^{-1} in the IR and Raman spectra of BMBP is predicted at 1400 cm^{-1} and is red shifted by 5 and 8 cm^{-1} with larger intensity in the CMBP and FMBP (see Figure 3). Similarly, we have also noticed that a strong band that predicted at 1222 cm^{-1} in BMBP (Figure 3) is red shifted significantly when the bromine atom is replaced with a chlorine or fluorine atom.

CH_2 group vibrations

The CH_2 group basically contains six fundamental vibrations, such as, CH_2 symmetric stretch; CH_2 asymmetric stretch; CH_2 scissoring and CH_2 rocking, CH_2 scissoring and CH_2 rocking. Normally, CH_2 asymmetric and symmetric stretching vibrations occur in the region 3000 ± 45 cm^{-1} and 2950 ±45 cm^{-1} [36-38]. In the present study the mode corresponds to the CH_2 symmetric vibration that is observed at 2918 cm^{-1} as a medium strong band in the FT-Raman spectrum and its counterpart in the FT-IR spectrum is not observed. However, the band that corresponds to the CH_2 asymmetric vibration is not observed either in the FT-IR or the FT-Raman spectrum. This vibration is assigned to the calculated frequency 2793 cm^{-1} on the basis of the PED contribution. However, in the case of CMBP and FMBP these vibrations are predicted in same region as that of BMBP. The CH_2 scissoring vibration is observed as a medium strong band at 1438 cm^{-1} in FT-IR spectra. This vibration is red shifted with increasing electronegativity of the halogen substituent. For instance, this vibration is predicted at 1464 and 1479 cm^{-1} in CMBP and FMBP. The strong and medium band observed at 1226 and 1133 cm^{-1} in FT-IR spectrum is assigned to CH_2 wagging and CH_2 twisting vibrations and their counterparts in the FT-Raman spectrum are not observed. These vibrations have a dominating contribution from the C-H in-plane bending vibration. Based on the PED analysis and visual inspection with Gauss View the CH_2 rocking mode is assigned to the observed frequency 882 cm^{-1} in the FT-IR spectrum. In CMBP and FMBP, this vibration is assigned to the calculated frequencies 904 and 1026 cm^{-1}.

C≡N group vibrations

The C≡N stretching vibration generally appears as a strong band in the FT-IR and FT-Raman spectra around 2000 ± 50 cm^{-1} in benzonitrile derivatives [17]. This vibration is mostly not effected by the other substituents in the ring. For instance, in 4-methyl-2-cyanobiphenyl this vibration is observed as a strong band both in the FT-IR and FT-Raman spectra at 2225 cm^{-1}. For BMBP, we have observed this vibration as a strong band both in the FT-IR and FT-Raman spectra at 2219 and 2224 cm^{-1}, respectively. The PED indicates that this frequency is pure and separated from the other ones. It mixes with the C-CN stretching mode to the extent of 11%. The calculated results agree also well with the experimental data. The C≡N in-plane bending vibration is assigned to a medium strong band in the FT-Raman spectrum at 140 cm^{-1}. This vibration is well confirmed from the PED and visual inspection by Gauss View. However, in the case of CMBP / FMBP, the C≡N stretching vibration and the C≡N in-plane bending vibration are predicted at 2247 / 2247 cm^{-1} and 143 / 139 cm^{-1}.

C-C≡N group vibrations

Normally in the benzonitrile molecule the C-C≡N stretching vibration occurs in the region 1100-1200 cm^{-1} [17]. For BMBP, this vibration is observed as a medium strong band at 1166 cm^{-1} (predicted at 1171 cm^{-1}) in the FT-Raman spectrum. The calculated PED results indicate that this frequency also has a contribution from the C-C ring stretching and in-plane C-H bending vibrations. Whereas, in CMBP and FMBP this vibration is assigned to the predicted frequency 1176 cm^{-1}. The C-C≡N in-plane bending vibration generally appears in the region 550±45 cm^{-1}. Recently, Sebastian et al. [17] reported the C-C≡N in-plane bending vibration of 4-methyl-2-cyanobiphenyl at 600 cm^{-1} in the FT-IR spectrum. For the BMBP this vibration is observed at 526 and 536 cm^{-1} in the FT-IR and FT-Raman spectra with weak intensity. However, this vibration is predicted at 542 and 545 cm^{-1} in CMBP and FMBP. The weak band observed at 169 cm^{-1} in FT-Raman spectrum is assigned to the C-C≡N out-of-plane bending vibration on the basis of visual inspection by Gauss View.

C-X (X = Br, Cl, F) group vibrations

In bromo substituted benzene derivatives the C-Br stretching frequency usually occurs in the region 500-700 cm^{-1} [36-38]. The strong band at 607 cm^{-1} in the FT-IR spectrum of BMBP is assigned to the C-Br stretching vibration. The H-C-Br in-plane bending vibration is not observed experimentally but on the basis of PED analysis we have assigned this vibration

to the calculated frequency 85 cm^{-1}. Generally, C-F and C-Cl stretching vibrations occurs in the region 1000-1400 cm^{-1} and 600-800 cm^{-1}. However, in the present study we have predicted the C-F stretching vibration at 1043 cm^{-1} in the theoretical IR spectrum of FMBP on the basis of the PED contribution. It is important to note that this band does not appear in CMBP and BMBP. Also, the band that appeared at 652 cm^{-1} in the simulated IR and Raman spectra of CMBP is pertains to the C-Cl stretching vibration.

4.3. Thermodynamic properties

The thermodynamic properties, such as heat capacity ($C^{\circ}_{p,m}$), entropy (S°_{m}) and enthalpy (H°_{m}), for the title compounds on the basis of vibrational analysis were computed using (perl script) THERMO.PL [39] and are listed in Table S3. From Table S3, one can notice that the values of $C^{\circ}_{p,m}$, S°_{m} and H°_{m} for BMBP, CMBP and FMBP increase with increasing temperature from 100 to 500 K, which is attributed to the enhancement of the molecular vibration as the temperature increases. Table S3 also indicates that the entropy and heat capacity of the studied molecules decrease in the order BMBP > CMBP > FMBP. Whereas, the enthalpy is getting higher with the increasing electronegativity of the halogen atom.

4.4. Electronic absorption spectrum

In order to better understand the nature of the peaks observed in the UV–vis absorption spectra, the low-lying singlet excited states of the BMBP compound have been calculated at the CAM-B3LYP/6-31G(d,p) level by using the TD-DFT approach on the previously optimized ground-state geometry of the molecule are listed in Table S4. The experimental absorption spectra of the BMBP in dichloromethane and methanol are presented in Fig. 4(a). The calculated results (see Fig 4(b)) compare well with the experimental data (Fig. 4(a)) and validate the current method for predicting the absorption spectrum of CMBP and FMBP (see Figure S1). The absorption spectrum of the three molecules contains two main peaks, the first one in the range (210-240 nm) corresponds to the $\pi \rightarrow \pi^*$ transitions of the aromatic moieties. The second band (240-320 nm) is attributed to a transition involving the whole molecule associated with intramolecular charge transfer. For instance, the computed results of BMBP (Table S4) shows that the first excited state at 260 nm originates from the HOMO (highest occupied molecular orbital) to LUMO (lowest unoccupied molecular orbital) transition that corresponds to the λ_{max} absorption band in the absorption spectrum. The second transition at 220 nm with lower oscillator strength originated from H-2->LUMO (34%), HOMO->L+1 (19%).

Figure 4

The most representative HOMO and LUMO plots of the title compounds in the ground state were shown in Figure S2. From Figure S1, one can see that the HOMO and LUMO of the title compounds were completely localized on entire molecule. This indicates that the HOMO→LUMO transition is providing a dominating contribution to the intramolecular charge transfer (ICT) characteristic. The π→π* transitions are mainly assigned to the characteristic orbitals that are transferred between benzonitrile and (bromomethyl)benzene moieties.

From Table S4 we can also notice that the λ_{max} highly depends upon solvent polarity. It was observed that the wavelength shifts towards shorter wavelengths when the solvent was changed from dichloromethane (ε = 9.1) to methanol (ε = 33). The hypsochromic shifting of the bands occurred due to difference in the stabilization of ground and excited states and thus causes a change in energy gap between these electronic states. This leads to a change in charge distribution and delocalization of electrons. Thus, both the ground and the excited n→π* transition does not occur in the molecules as the lone pair of electrons on the nitrogen atom cannot be forced to overlap maximally due to the rigidity of the ring system of the molecules. Finally, the calculated results indicate that the molecular extinction coefficient of the charge transfer peak is decreasing with increasing electronegativity of the halogen substituent (see Fig. 4 and S1).

4.5.Global chemical reactivity descriptors

The global chemical reactivity descriptors play an important role in understanding the global nature of molecules in terms of their stability and reactivity [40]. Global chemical reactivity descriptors such as hardness, chemical potential, softness, electronegativity and electrophilicity index are mainly governed by the HOMO and LUMO energy levels. These parameters can be calculated using DFT methods. In order to understand how these parameters vary upon replacing the bromine atom in BMBP with chlorine and fluorine atoms, which leads to the structures CMBP and FMBP, we have computed the HOMO and LUMO energies, the energy gap (ΔE), the ionization potential (I), the electron affinity (A), the absolute electronegativity (χ), the absolute hardness (η) and softness (σ) of the investigated molecules using B3LYP / 6-31G(d,p) method and the results are presented in Table S5.

According to Koopman's theorem, the electronegativity (χ), chemical potential (μ) and chemical hardness (η) for a closed shell molecule can be defined as [40]:

$$\chi = [I + A] / 2 = - [E_{LUMO} + E_{HOMO}] / 2$$

$$\eta = [I - A] / 2 = - [E_{LUMO} - E_{HOMO}] / 2$$

$$\mu = - \chi$$

where I and A are the ionization potential and electron affinity, $I = -E_{HOMO}$ and $A = -E_{LUMO,}$ respectively as shown in Table S5.

Generally, μ and η are related to the charge transfer characteristic and stability of the system. The calculated results indicate that η decreases with increasing electronegativity of the halogen substituent. The stability of the investigated molecules varies as BMBP > CMBP > FMBP. On the other hand, Parr et al. proposed an electrophilicity index (ω) as a measure of energy lowering due to maximal electron flow between donor and acceptor. The effectiveness of this new reactivity quantity has been proven to give information about the toxicity of various pollutants in terms of their reactivity and site selectivity [40]. The calculated results indicate that ω is increasing with decreasing energy gap of the molecules. Normally, a molecule with low energy gap means that it is more reactive. From Table S5 one can notice that the energy gap of the molecules decreases in the order BMBP > CMBP > FMBP. This indicates that the hardness and global softness (σ) of the BMBP molecule are decreasing and increasing with increasing electronegativity of the halogen atom.

4.6. Nonlinear optical properties

Generally, conjugated organic molecules are the most constructive materials for optoelectronic devices. Since the advent of nonlinear optics, there has been a long and sustained interest in organic materials with significant nonlinear optical (NLO) properties. Therefore, in order to measure the SHG efficiency of BMBP, urea crystals grounded into an identical size as that of the sample were used as the reference material. We did not detect any SHG with an incident wavelength of 532 nm for BMBP. It is possible that this material does show nonlinear optical SHG activity but at di□erent incident wavelengths. In order to verify this, the static and dynamic molecular hyperpolarizabilities of the BMBP molecule along with the CMBP, FMBP and urea molecules were computed using quantum chemical calculations and are presented in Table S6.

The calculated first hyperpolarizability value of urea in water solvent (β_{total} = 70 au) at λ = 1064 nm at the B3LYP/6-31G(d,p) level is in good agreement with the experimental data [41]. Therefore, we have adopted current method to investigate the static and dynamic hyperpolarizabilities of title compounds. The calculated results show that the static and dynamic first hyperpolarizability values of BMBP are smaller than those of urea. Whereas, for CMBP and FMBP the dynamic first hyperpolarizability is 1.54 and 12.54 times higher

than that of the urea. Among all the investigated molecules in this paper FMBP has the largest first hyperpolarizability. The first hyperpolarizability of the compounds in increasing order is BMBP< CMBP < FMBP. This indicates that the first hyperpolarizability of the BMBP will increase when the electronegativity of the substituent group on the phenyl ring B is increasing.

5. Conclusions

In this paper the vibrational and electronic properties of 4′-halomethyl-2-biphenylcarbonitrile compounds were determined for the first time. Due to unavailability of CMBP and FMBP, we have done complete vibrational and electronic spectra studies to BMBP. Based on these results we have investigated the influence of the halogen substituent on the spectral characteristics. The results obtained in this study will certainly useful for the further studies of these derivatives.

A complete vibrational and molecular structure analysis has been performed based on the quantum mechanical approach by normal coordinate analysis and density functional theory calculation. The difference between the observed and scaled wavenumber values of most of the fundamentals is very small for BMBP. The theoretically simulated FT-IR and FT-Raman spectrum shows good correlation with the experimentally observed FT-IR and FT-Raman spectrum. Therefore, the assignments made at the DFT level of theory with reasonable deviations from the experimental values seem to be correct and validates the current method for predicting the vibrational spectra of CMBP and FMBP. The dihedral angle between the two phenyl rings A and B of BMBP/ CMBP/ FMBP is 48.23° / 47.55° / 46.92° , respectively as is evident from the optimized structure. The TDDFT calculated results of BMBP is in good agreement with the experimental data. This indicates that the predicted absorption spectra of CMBP and FMBP are valid and acceptable. The results also indicate that for the three molecules the HOMO→LUMO transition corresponds to the intramolecular charge transfer (ICT) characteristic and the $\pi \rightarrow \pi^*$ transition to the characteristic orbitals that are transferred between the benzonitrile and (bromomethyl)benzene moieties. The energy gap of the BMBP molecule is decreasing with increasing electronegativity of the halogen atom. Finally, our results also indicate that the first dynamic hyperpolarizability of the BMBP is increasing as the electronegativity of the substituent group on the phenyl ring B is increasing.

References

[1]. W. Z. Yuan, F. Mahtab, Y. Gong, Z. Q. Yu, P. Lu, Y. Tang, J. W. Y. Lam, C. Zhu, B. Z. Tang, Synthesis and self-assembly of tetraphenylethene and biphenyl based AIE-active triazoles, J. Mater. Chem., 22 (2012) 10472–10479.

[2]. M. A. Wahab, C. He, Self-Assembly, Optical, and Mechanical Properties of Surfactant-Directed Biphenyl-Bridged Periodic Mesostructured Organosilica Films with Molecular-Scale Periodicity in the Pore Walls, Langmuir, 25 (2009) 832–838.

[3]. L. P. Hao, W. Z. Xue, X. F. Han, X. He, J. Zhang, Z. M. Zhou, Design, synthesis and biological activity of 4′-[(benzimidazol-1-yl)methyl]biphenyl-2-sulphonamides as dual angiotensin II and endothelin A receptor antagonists, Med. Chem. Commun., 6 (2015) 715-718.

[4]. N. Murugesan, J. E. Tellew, Z. Gu, B. L. Kunst, L. Fadnis, L. A. Cornelius, R. A. F. Baska, Y. Yang, S. M. Beyer, H. Monshizadegan, K. E. Dickinson, B. Panchal, M. T. Valentine, S. Chong, R. A. Morrison, K. E. Carlson, J. R. Powell, S. Moreland, J. C. Barrish, M. C. Kowala and J. E. Macor, Discovery of N-isoxazolyl biphenylsulfonamides as potent dual angiotensin II and endothelin A receptor antagonists, J. Med. Chem., 45 (2002) 3829-3835.

[5]. J D McKinney, L G Pedersen, Biological activity of polychlorinated biphenyls related to conformational structure, Biochem J, 240 (1986) 621–622.

[6]. J.D. Mckinney, P. Singh, Structure-activity relationships in halogenated biphenyls: unifying hypothesis for structural specificity , Chem.Biol Interactions, 33 (1981) 271-283.

[7]. D. Steele, E. R. Lippincott, The crystal and solution vibrational spectra of biphenyl, J. Mol. Spec., 6 (1961) 238-264.

[8]. R. J. Pulham, D. Steele, Vibrational spectra of 4, 4′-difluorobiphenyl-d8 and the structure of biphenyls in solution, J. Raman. Spec., 15 (1984) 217-223.

[9]. R. M. Barrett, D. Steele, The vibrational spectra and dihedral angles of biphenyl and the 4,4'-dihalogenobiphenyls, J. Mol. Structure, 11 (1972) 105-125.

[10]. R. M. Barrett, D. Steele, The vibrational spectra of d_{10} and 4,4′ d_2 biphenyl , Spectrochimica acta A, 30 (1974) 1731- 1738.

[11]. S. Y. Lee, Bull. Korean. Chem. Soc. 19 (1998) 93-98.

[12]. H. C. Hsu, Y. Dyakov, C-K. Ni, Energy transfer of highly vibrationally excited biphenyl., J. Chem. Phys., 133 (2010) 174315.

[13]. G. Zerbi, S. Sandroni, Fundamental frequencies and molecular configuration of biphenyl—I. Re-analysis of its vibrational spectrum, Spectrochimica acta A, 24 (1968) 483-510.

[14]. R. Fukuda , M. Ehara, Electronic excited states and electronic spectra of biphenyl: a study using many-body wavefunction methods and density functional theories, Phys. Chem. Chem. Phys., 15 (2013) 17426-17434.

[15]. R. Grinter, The electronic spectra of diphenyl and its sterically hindered derivatives, Molecular Physics, 11 (1966) 7-15.

[16]. Y. Takei, T. Yamaguchi, Y. Osamura, K. Fuke, and K. Kaya, Electronic spectra and molecular structure of biphenyl and para-substituted biphenyls in a supersonic jet, J. Phys. Chem. 92 (1988) 577-581.

[17]. S. Sebastian, N. Sundaraganesan, B. Karthikeiyan, V. Srinivasan, Quantum mechanical study of the structure and spectroscopic (FT-IR, FT-Raman, ^{13}C, ^{1}H and UV), first order hyperpolarizabilities, NBO and TD-DFT analysis of the 4-methyl-2-cyanobiphenyl, Spectrochimica Acta Part A, 78 (2011) 590–600.

[18]. A. Imamura, R. Hoffmann, Electronic structure and torsional potentials in ground and excited states of biphenyl, fulvalene, and related compounds, J. Am. Chem. Soc. (1968) 5379-5385.

[19]. T. Hoshi, H. Inoue, J. Shiraishi, Y. Tanizaki, Electronic Spectra of Biphenyl and Fluorene, Bull. Chem. Soc. Jap, 44 (1971) 1743-1745.

[20]. T. Yoshinaga, H. Hiratsuka, Y. Tanizaki, Polarized Electronic Absorption Spectra and Assignment of Fluorene and Biphenyls, Bull. Chem. Soc. Jap, 51 (1978) 996-1000.

[21]. H. M. L. Dieteren, C. Koningsberger, A study of some biphenylamines†: Part I. The electronic spectra in acidic solvents of some biphenylamines, RECUEIL, 82 (1963) 5-16.

[22]. Y. Gondo, Electronic Structure and Spectra of Biphenyl and Its Related Compound, J. Chem. Phys., 41 (1964) 3928-3938.

[23]. T. G. Mclaughlin, L. B. Clark, The electronic spectrum of biphenyl, Chem. Phys., 31 (1978) 11-18.

[24]. B. Tinland, A theoretical study of the ultraviolet absorption spectra of biphenyl, Acta Physica Academiae Scientiarum Hungaricae, 1968, 25, 111-114.

[25]. M. Schmitt, M. Bohm, C. Ratzer , S. Siegert , M. van Beek , W. L. Meert, Electronic excitation in the benzonitrile dimer: The intermolecular structure in the S0 and S1 state determined by rotationally resolved electronic spectroscopy, J. Mol. Structure, 795 (2006) 234–241

[26]. I. B. Berlman and O. J. Steingraber, Further Evidence of a Hidden Singlet Transition in Biphenyl, J. Chem. Phys. 43 (1965) 2140.

[27]. M. Karabacak, E. Yilan, Molecular structure, spectroscopic (FT-IR, FT-Raman, 13C and 1H NMR, UV), polarizability and first-order hyperpolarizability, HOMO and LUMO analysis of 4′-methylbiphenyl-2-carbonitrile, Spectrochim. Acta A 87 (2012) 273-285

[28]. M.Kaur, Y.S. Mary, H.T. Varghese, C. Y. Panicker, H.S. Yathirajan, M.S. Siddegowda, C. Van Alsenoy, Vibrational spectroscopic, molecular structure, first hyperpolarizability and NBO studies of 4′-methylbiphenyl-2-carbonitrile, Spectrochim. Acta A 98 (2012) 91-99

[29]. J. V. Duncia, M. E. Pierce, J. B. III. Santell, Three synthetic routes to a sterically hindered tetrazole. A new one-step mild conversion of an amide into a tetrazole, J. Org. Chem. 56 (1991) 2395-2400.

[30]. Q. B. Song, Y. Z. Li, C. Z. Qi, T. H. Shen, H. B. Wang, 4'-Bromomethylbiphenyl-2-carbonitrile, Acta Cryst. E59 (2003) o1944-o1945.

[31]. M.J. Frisch et al., GAUSSIAN09, Revision A.02, Gaussian Inc., Wallingford, CT, 2009.

[32]. C. Lee, W. Yang, R.G. Parr, Development of the Colle-Salvetti correlation-energy formula into a functional of the electron density, Phys. Rev. B, 37 (1988) 785.

[33]. G. Keresztury, J. M. Chalmers, P. R. Griffith (Eds.), Raman Spectroscopy: Theory, Hand book of Vibrational Spectroscopy, vol. 1, John Wiley & Sons Ltd.: New York, 2002.

[34]. G. Fogarasi, P. Pulay, J.R. Durig (Eds.), Vibrational Spectra and Structure, vol. 14, Elsevier, Amsterdam, 1985.

[35]. T. Sundius, J. Mol. Struct. 1990, 218, 321. MOLVIB: A Program for Harmonic Force Field Calculations, QCPE program No. 604 (1991).

[36]. G. Socrates, Infrared and Raman Characteristic Group Frequency, third ed., Wiley, New York, 2001.

[37]. L.J. Bellamy, The Infrared Spectra of Complex Molecules, third ed., Wiley, New York, 1975.

[38]. G. Varsanyi, Assignments for Vibrational Spectra of Seven Hundred Benzene Derivatives, vols. 1 and 2, Academiai Kiado, Budapest, 1973.

[39]. K.K. Irikura, THERMO.PL, National Institute of Standards and Technology, 2002

[40]. R. Vijayaraj, V. Subramanian, P. K. Chattaraj, Comparison of Global Reactivity Descriptors Calculated Using Various Density Functionals: A QSAR Perspective, J. Chem. Theory Comput. 5 (2009) 2744–2753.

[41]. I. Ledoux and J. Zyss, Influence of the molecular environment in solution measurements of the Second-order optical susceptibility for urea and derivatives, Chem. Phys., 73, 203, 1982.

Table captions

Table 1. Optimized geometrical parameters of 4′-halomethyl-2-biphenylcarbonitrile compounds obtained by B3LYP/6-31G(d,p) density functional calculations.

Table 2: Detailed assignments of fundamental vibrations of BMBP, CMBP and FMBP by normal mode analysis based on SQM force field calculations using B3LYP/6-31G(d,p)

Figure captions

Figure 1 Molecular structure of 4′-halomethyl-2-biphenylcarbonitrile compounds along with numbering of atom.

Figure 2 Experimental and simulated (a) FT-IR and (b) FT-Raman spectra of BMBP

Figure 3 Simulated (a) FT-IR and (b) FT-Raman spectra of BMBP, CMBP and FMBP.

Figure 4 (a) Experimental and (b) theoretical UV-visible spectra of BMBP in dichloromethane and methanol.

Supplementary material captions

Table S1. Definition of internal coordinates of 4′-halomethyl-2-biphenylcarbonitrile

Table S2. Definition of local-symmetry coordinates and the values of corresponding scale factors used to correct the B3LYP/6-31G(d,p) (refined) force field of 4′-halomethyl-2-biphenylcarbonitrile compounds.

Table S3 Thermodynamic properties for the title compounds obtained by B3LYP/6-31 G (d, p) density functional calculations

Table S4. Main calculated (CAM-B3LYP with 6-31G (d,p) basis set) optical transitions for BMBP, CMBP and FMBP in DCM and methanol.

Table S5. Quantum chemical parameters for the title compounds obtained by B3LYP/6-31 G (d, p) density functional calculations

Table S6. First order hyperpolarizability (β) components of title compounds and urea. All the values are in a.u.

Figure S1. Theoretical UV-visible spectra of (a) CMBP and (b) FMBP in dichloromethane and methanol.

Figure S2. HOMO and LUMO orbitals in the optimized ground state structure of BMBP, CMBP and FMBP calculated at the CAM-B3LYP/6-31G(d,p) level.

Table 1. Optimized geometrical parameters of 4′-halomethyl-2-biphenylcarbonitrile compounds obtained by B3LYP/6-31G(d,p) density functional calculations.

Bond length (Å)	Calculated			Exp[a]	Bond angle (°)	Calculated			Exp[a]
	BMBP	CMBP	FMBP	BMBP		BMBP	CMBP	FMBP	BMBP
C_1-C_2	1.417	1.416	1.417	1.407	C_1-C_2-C_3	120.674	120.638	120.688	120.212
C_2-C_3	1.407	1.406	1.406	1.405	C_2-C_3-C_4	120.457	120.467	120.490	120.170
C_3-C_4	1.391	1.390	1.389	1.368	C_3-C_4-C_5	119.461	119.482	119.438	120.318
C_4-C_5	1.397	1.395	1.395	1.363	C_4-C_5-C_6	120.222	120.226	120.239	120.648
C_5-C_6	1.394	1.393	1.392	1.388	C_5-C_6-C_1	121.696	121.697	121.767	120.960
C_6-C_1	1.404	1.403	1.403	1.395	C_6-C_1-C_2	117.482	117.486	119.655	117.667
C_7-C_8	1.406	1.405	1.403	1.394	C_7-C_8-C_9	120.802	120.852	121.094	120.287
C_8-C_9	1.392	1.391	1.392	1.388	C_8-C_9-C_{10}	120.692	120.666	120.338	120.222
C_9-C_{10}	1.401	1.400	1.396	1.387	C_9-C_{10}-C_{11}	118.612	118.617	118.970	119.072
C_{10}-C_{11}	1.401	1.399	1.399	1.355	C_{10}-C_{11}-C_{12}	120.875	120.882	120.732	121.824
C_{11}-C_{12}	1.392	1.391	1.391	1.390	C_{11}-C_{12}-C_7	120.653	120.648	120.692	119.726
C_{12}-C_7	1.404	1.403	1.404	1.382	C_{12}-C_7-C_8	118.359	118.332	118.168	118.866
C_1-C_7	1.486	1.486	1.485	1.486	C_2-C_1-C_7	122.901	122.925	122.968	122.477
C_{10}-C_{15}	1.490	1.498	1.508	1.498	C_1-C_7-C_{12}	121.638	121.763	121.759	121.082
C_2-C_{13}	1.436	1.435	1.435	1.400	C_9-C_{10}-C_{15}	120.634	120.700	120.872	120.554
$C_{13}\equiv N_{14}$	1.164	1.163	1.163	1.155	C_{10}-C_{15}-X_{16}	111.575	112.339	111.147	113.259
C_{15}-X_{16}	2.001	1.839	1.389	1.958	C_2-$C_{13}\equiv N_{14}$	177.253	177.376	177.260	177.688
Energy (Hartees)	-3166.025	-1054.473	-694.104						

[a] See ref 28

Table 2: Detailed assignments of fundamental vibrations of BMBP, CMBP and FMBP by normal mode analysis based on SQM force field calculations using B3LYP/6-31G(d,p)

	BMBP						CMBP				FMBP			
S.No	**ν_{scaled} (cm^{-1})**	**ν_{IR} (cm^{-1})**	**ν_{Raman} (cm^{-1})**	**I_{IR}[a]**	**I_{RA}[b]**	**Characterization of normal modes with PED (%)**	**ν_{scaled} (cm^{-1})**	**I_{IR}[a]**	**I_{RA}[b]**	**Characterization of normal modes with PED (%)**	**ν_{scaled} (cm^{-1})**	**I_{IR}[a]**	**I_{RA}[b]**	**Characterization of normal modes with PED (%)**
1	3087		3088 m	0.169	10.40	VCH (99)	3088	0.226	15.50	VCH (99)	3092	0.156	24.50	VCH (99)
2	3082			0.185	8.80	VCH (99)	3085	0.229	13.80	VCH (99)	3088	0.233	31.00	VCH (99)
3	3078		3060 vs	0.202	7.44	VCH (99)	3080	0.250	10.30	VCH (99)	3084	0.241	24.20	VCH (99)
4	3072			0.181	6.73	VCH (99)	3073	0.231	10.10	VCH (99)	3079	0.229	17.10	VCH (99)
5	3069			0.177	6.21	VCH (99)	3071	0.226	9.65	VCH (99)	3072	0.141	13.70	VCH (99)
6	3060			0.170	4.73	VCH (99)	3061	0.201	7.17	VCH (99)	3062	0.136	10.80	VCH (99)
7	3058			0.184	4.62	VCH (99)	3059	0.222	7.23	VCH (99)	3060	0.137	10.90	VCH (99)
8	3052		3039 m	0.166	3.40	VCH (99)	3053	0.196	5.38	VCH (99)	3045	0.184	8.42	VCH (99)
9	2853	3028 m		0.007	1.60	VCH2as (100)	2840	0.047	3.05	VCH2as (100)	2743	0.391	12.10	VCH2as (98)
10	2793		2918 m	0.085	3.94	VCH2ss (100)	2782	0.190	6.07	VCH2ss (100)	2706	0.449	28.60	VCH2ss (97)
11	2235	2219 s	2224 s	0.349	19.50	VCN (89), VCC3 (11)	2247	0.264	21.80	VCN (89), VCC3 (11)	2247	0.259	40.70	VCN (89), VCC3 (11)
12	1602		1614 s	0.025	100.00	VCC2 (62), βCH (22)	1608	0.035	100.00	VCC2 (63), βCH (22)	1612	0.031	100.00	VCC2 (63), βCH (22)
13	1584	1591 m	1597 s	0.125	38.60	VCC1(62), βCH (22)	1591	0.112	45.20	VCC (62), βCH (22)	1591	0.134	68.00	VCC1 (62), βCH (22)
14	1559	1559m	1578 m	0.027	8.51	VCC2 (40), VCC1 (28), βCH (14)	1566	0.021	10.20	VCC2 (39), VCC1 (29), βCH (14)	1567	0.016	15.10	VCC2 (44), VCC1 (24), βCH (13)
15	1544	1518 w	1518 m	0.034	6.25	VCC1 (41), VCC2 (27), βCH (18)	1551	0.040	6.74	VCC1 (40), VCC2 (28), βCH (18)	1552	0.064	12.00	VCC1 (45), VCC2 (22), βCH (19)
16	1504			0.017	4.30	βCH (53), VCC2 (31), VCC3 (12)	1509	0.018	8.04	βCH (53), VCC2 (31), VCC3 (12)	1510	0.045	26.60	βCH (52), VCC2 (31), VCC3 (12)

17	1466	1473 s	1481 w	0.320	11.70	βCH (52), VCC1 (34)	1471	0.337	15.00	βCH (51), VCC1 (35)	1479	0.132	15.50	βCH2 (81)
18	1458			0.116	4.63	βCH2 (94)	1464	0.135	7.53	βCH2 (94)	1471	0.417	21.60	βCH (51), VCC1 (35), VCC3 (6)
19	1431	1438 s	1438w	0.087	3.74	βCH (58), VCC1 (28)	1438	0.091	4.33	βCH (57), VCC1 (28)	1437	0.068	8.77	βCH (56), VCC1 (28)
20	1400	1404 m	1380 w	0.101	0.56	βCH (48), VCC2 (39)	1405	0.123	0.68	βCH (48), VCC2 (39)	1407	0.330	5.65	βCH (35), VCC2 (28), βCH2 (14)
21	1317	1324 w	1303 s	0.009	1.51	βCH (62), VCC2 (26)	1320	0.015	1.83	βCH (61), VCC2 (26)	1377	0.416	10.60	VCC2 (26), βCH (25), βCH2 (22)
22	1295			0.026	9.97	VCC2 (60), βCH (18)	1298	0.038	11.10	VCC2 (61), βCH (19)	1303	0.036	9.71	βCH (68), VCC1 (11), VCC2 (10)
23	1285	1268m	1260 m	0.027	27.90	VCC1 (63), βCH (18), VCC3 (11)	1287	0.068	30.20	VCC1 (64), βCH (17), VCC3 (10)	1290	0.099	48.40	VCC2 (51), βCH (21)
24	1258			0.112	16.10	VCC1 (40), VCC2 (24), βCH (19)	1267	0.931	30.40	βCH2 (35)	1287	0.103	54.30	VCC1 (57), VCC2 (20), βCH (11)
25	1238			0.153	22.00	βCH (39), VCC1 (25), VCC3 (17)	1260	0.341	31.90	VCC1 (38), VCC2 (24), βCH (19), VCC3 (10)	1259	0.079	38.50	VCC1 (36), VCC2 (31), βCH (15), VCC3 (10)
26	1224	1226 s		1.000	57.00	βCH2 (28), VCC3 (18)	1241	0.042	28.20	βCH (39), VCC1 (25), VCC3 (18)	1240	0.035	44.30	βCH (40), VCC1 (24), VCC3 (17)
27	1201		1215 w	0.095	25.30	VCC3 (36), VCC2 (25), βCH (12), βR2tri (10)	1198	0.119	27.50	VCC3 (39), VCC2 (28), βCH (17), βR2tri (11)	1234	0.048	24.60	βCH (65), βCH2 (27)
28	1180	1187	1188 m	0.027	33.80	βCH (73), VCC2 (19)	1183	0.028	34.30	βCH (70), VCC2 (18)	1196	0.048	8.03	VCC2 (33), VCC3 (29), βCH (24)
29	1171		1166 m	0.024	18.70	VCC3 (33), VCC1 (27), βCH (20), βR1tri (15)	1176	0.024	22.20	VCC3 (33), VCC1 (27), βCH (20), βR1tri (15)	1176	0.027	44.50	VCC3 (29), βCH (27), VCC1 (23), R1tri (11)
30	1158	1159 m		0.018	6.98	βCH (80), VCC1 (20)	1161	0.014	8.75	βCH (80), VCC1 (20)	1175	0.028	42.90	βCH (52), VCC3 (18), VCC2 (15)
31	1130	1133 m		0.008	1.40	βCH (32), VCC2 (25), βCH2 (23)	1145	0.006	4.10	βCCl (33), βCH2 (28), VCC2 (21), βCH (16)	1161	0.015	14.00	βCH (80), VCC1 (19)
32	1100	1106 m		0.043	1.18	βCH (31), VCC2 (19), VCC1 (13),	1110	0.042	1.16	βCH(45), VCC2 (29)	1115	0.042	1.10	βCH (54), VCC2 (32)
33	1090			0.050	1.05	βCH (29), VCC1 (26), VCC2 (16)	1096	0.025	0.93	VCC1 (33), βCH (31), βR1tri (10), VCC2 (10)	1096	0.013	1.13	VCC1 (36), βCH (30)
34	1034	1044 w	1049 m	0.026	15.40	VCC1 (55), βCH (20), βR1tri (12)	1038	0.017	15.90	VCC1 (56), βCH (21), βR1tri (11)	1043	1.000	17.20	VCF (82)
35	1008			0.014	1.45	VCC2 (41), βR2tri (27), βCH (14)	1011	0.009	1.96	VCC2 (41), R2tri (24), βCH (14), VCC1 (12)	1039	0.621	27.30	VCC1 (57), βCH (21),
36	990	1002 m		0.121	1.97	γCH (85), τR1tri (12)	991	0.105	2.71	R2tri (40), R1tri (24), VCC1 (20), VCC2 (15)	1026	0.100	4.32	βCH2 (43), γCH (17)

37	989			0.093	2.00	βR2tri (35), βR1tri (25), VCC1 (23), VCC2 (16)	987	0.067	1.99	γCH (85), τR1tri (12)	1009	0.053	3.08	VCC2 (41), βR2tri (20), VCC1 (13), βCH (13)
38	971			0.020	1.39	γCH (91)	962	0.018	2.61	γCH (85)	990	0.093	4.34	R2tri (41), R1tri (22), VCC1 (18), VCC2 (16)
39	967			0.019	1.20	γCH (74)	960	0.020	2.78	γCH (85)	987	0.074	3.60	γCH (85), τR1tri (12)
40	960	953 m		0.023	0.62	γCH (89)	954	0.023	1.44	γCH (88)	965	0.023	2.60	γCH (89)
41	887			0.022	1.16	γCH (69)	904	0.006	1.52	βCH2 (38), βCCl (27), VCC2 (13)	956	0.024	2.57	γCH (88)
42	882	882 s		0.021	0.99	γCH (30), βCBr (24), βCH2 (21)	889	0.012	3.32	γCH (77)	952	0.023	2.22	γCH (86)
43	848	833 s		0.277	2.27	γCH (71)	850	0.207	3.21	γCH (71)	888	0.009	5.90	γCH (78)
44	840		825 w	0.094	4.19	γCH (98)	843	0.078	6.87	γCH (99)	850	0.048	9.96	γCH (97)
45	811		810 m	0.136	4.01	VCC2 (28), VCC3 (18), τR2tri (12)	809	0.182	6.33	VCC2 (31), VCC3 (22), βR2sym (13)	829	0.262	4.91	γCH (71)
46	784		783 m	0.102	2.11	τR2tri (57), γCCme (10)	775	0.418	4.65	τR2tri (35), γCH (30)	805	0.080	19.40	VCC2 (29), VCC3 (22), βR2sym (14)
47	768		770 w	0.587	4.03	γCH (51), βR1asy (11),	771	0.483	4.89	γCH (45)	772	0.548	18.50	γCH (70)
48	764	758 vs		0.552	4.87	γCH (29), τR1tri (24), γCCb (15)	766	0.290	5.34	τR1tri (32), γCCb (19), βCN1 (10)	769	0.452	22.90	τR1tri (18), βR1asy (14), VCC3 (14)
49	747	724 s		0.224	0.75	τR1tri (41), γCCb (19), τR2tri (12), γCH (11)	742	0.263	1.72	τR2tri (29), τR1tri (27), γCCb (11), γCH (11)	757	0.230	4.99	τR1tri (41), γCCb (22), γCH (11)
50	675	684 s	681 w	0.118	14.40	βR1sym (38), VCC3 (18), VCC1 (17)	677	0.254	24.40	βR1sym (37), VCC3 (18), VCC1 (16)	724	0.022	2.52	τR2tri (65), γCH (11)
51	636	641 s	642 w	0.020	4.39	βR2asy (55), βR2sym (24)	652	1.000	63.30	VCCl (50), τR2tri (12), γCH (11)	677	0.065	11.90	βR1sym (34), VCC3 (17), VCC1 (17)
52	601	607 s		0.426	27.80	γCCme (18), VCBr (14), γCH (12), τR2asy (12)	636	0.102	11.40	βR2asy (55), βR2sym (23)	635	0.004	9.01	βR2asy (47), βR2sym (29)
53	594			0.162	11.60	βR1sym (22), βCC (19), βR2asy (10)	597	0.035	14.00	βCC (23), β R1sym (20), βR2asy (10),	606	0.008	1.62	βR1sym (26), βR2asy (25), βCC (11)
54	577		564 w	0.091	11.10	βCN1 (35), βCN2 (28), τR1tri (11), τR1sym (10)	586	0.124	15.10	βCN1 (24)	584	0.062	8.13	βCN1 (41), βCN2 (23)
55	564	559 w		0.383	57.20	VCBr (33), βR2sym (11), βR1sym (10)	580	0.114	16.10	βCN2 (43), βCN1 (36)	580	0.050	9.23	βCN2 (47), βCN1 (26)

56	538	526 w	536 vw	0.146	18.50	βCN2 (26), βCN1 (20), γCCb (15)	542	0.052	5.52	βCN1 (35), βCN2 (22), γCCb (11)	545	0.037	5.77	βCN1 (32), βCN2 (17), γCCb (12)
57	503	503 m	508 w	0.032	7.87	βCCar (13), βCN1 (12), βR1asy (10)	505	0.041	5.15	βCN2 (25)	516	0.057	5.89	βCN2 (22), βCCar (11), βCN1 (10)
58	470	469 m	471 w	0.045	16.60	βR1asy (19),τR2asy (16), VCBr (13), VCC3 (10)	482	0.035	9.91	βR1asy (19), τR2asy (11), VCC3 (11)	475	0.058	10.20	τR2asy (18), γCCme (14), τR1asy (11)
59	418		414 w	0.005	12.80	τR2sym (62), τR2asy (18), γCH (16)	421	0.006	13.70	τR2sym (55), τR2asy (19), γCH (16)	428	0.032	17.20	τR2sym (14), βR1asy (12), VCC3 (12), τR2asy (10)
60	394		384 w	0.012	6.11	βCN1 (31), βCN2 (25), τR1sym (21), τR1asy (13)	398	0.024	9.32	βCN2 (37), βCN1 (37), τR1sym (13)	418	0.016	16.10	τR2sym (54), γCH (16), τR2asy (15)
61	376		351 w	0.042	12.00	βCN2 (19), βCCar (14), βCCme (13), βCN1 (10)	386	0.071	16.50	βCCar (17), βCN1 (12), βR1asy (11), τR2tri (10)	398	0.013	11.80	βCN1 (35), βCN2 (35), τR1sym (14)
62	344			0.052	12.40	βCCme (22), τR1asy (11),	351	0.030	4.15	βCN1 (20), βCCme (17), βCN2 (15), τR1asy (13)	361	0.009	14.00	βCCar (25), γCCme (19), βCN1 (13)
63	297		292 w	0.014	3.18	βCN2 (18), βCCme (15)	300	0.013	5.66	βCCme (20), βCCar (12), βCN1 (10)	320	0.005	14.40	βCN1 (20), τR1asy (20), βCN2 (16)
64	272		280 w	0.004	5.38	τR1asy (19), βCN1 (13)	272	0.007	10.40	βCN2 (19), βCN1 (16), τR1asy (14), βCCme (11)	257	0.007	26.00	VCC3 (17), βR2sym (16), βCN2 (11)
65	201		169 w	0.006	9.41	βCCar (15), τR2asy (11), βCN1 (11), γCCb (10)	220	0.013	12.70	βCN2 (14), τR2asy (14), βCCar (10)	203	0.090	14.30	βCCme (22), βCC (15), βCCar (13), βCN1 (13), βCF (11)
66	159		155 m	0.094	20.90	βCC (37), βCN2 (33)	165	0.105	23.80	βCC (42), βCN2 (21)	196	0.040	9.95	βCN2 (27), βCN1 (14), γCCb (11)
67	140		122 vs	0.026	9.46	βCN1 (38), βCN2 (29), γCCb (15)	143	0.021	18.60	βCN1 (41), βCN2 (39)	139	0.024	75.60	βCN1 (43), βCN2 (14)
68	98		98 s	0.014	87.10	τCC (57), βCCar (15)	101	0.014	111.00	γCCme (21), τCC (16), βCCl (15), βCCar (15), βCN2 (11)	134	0.028	68.50	βCN2 (47), βCN1 (23)
69	85			0.009	70.80	βCBr (23), γCCb (18), γCCme (17)	94	0.018	179.00	τCC (37), βCCar (13), γCCb (12)	87	0.009	282.00	τCC (40), βCCar (21), γCCb (11)
70	57			0.015	264.00	τCC (58), βCCar (12)	58	0.020	506.00	τCC (66)	62	0.065	642.00	τCC (46), γCCb (15), τR2asy (14)
71	36			0.037	258.00	τR2asy (23), γCH (16), γCC_{me} (16), γCCb (10)	44	0.028	219.00	τR2asy (25), γCH (16), γCCb (15), γCCme (13)	58	0.056	852.00	τCC (81)
72	33			0.039	285.00	τCC (89)	28	0.035	342.00	τCC (97)	31	0.049	482.00	τCC (97)

Abbreviations: ν, stretching; β, in plane bending; γ, out of plane bending; τ, torsion; tri, trigonal deformation; sym, symmetric deformation; asy, asymmetric deformation; vs, very strong; sh, shoulder; s, strong; ms, medium strong; w, weak; vw, very weak.

[a] Relative absorption intensities normalized with highest peak absorption equal to 1.

[b] Relative Raman intensities calculated by Eq. (1) and normalized to 100.

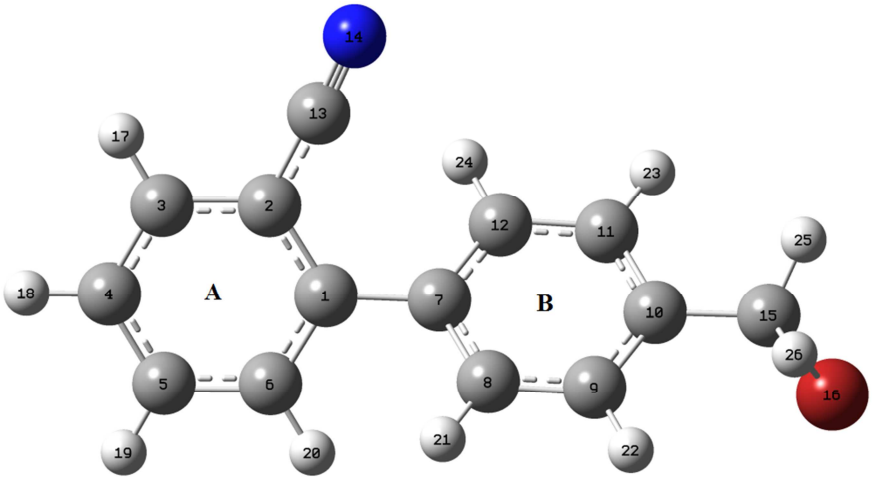

4′-bromomethyl-2-biphenylcarbonitrile (BMBP)

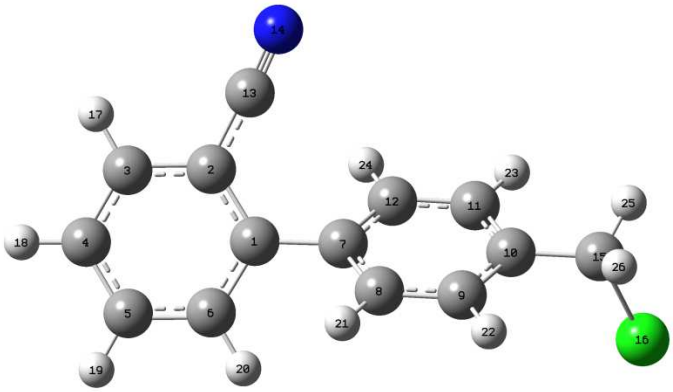

4′-chloromethyl-2-biphenylcarbonitrile (CMBP)

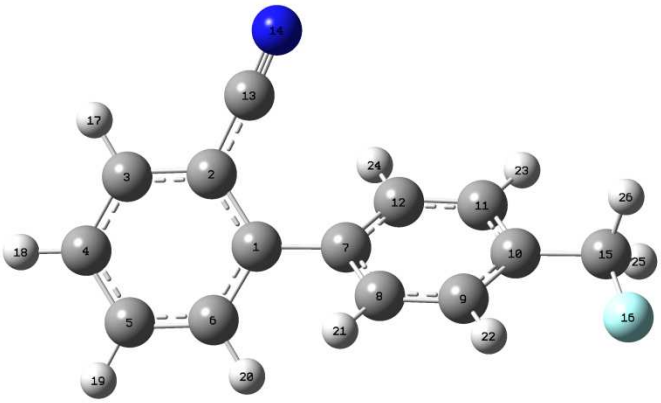

4′-fluoromethyl-2-biphenylcarbonitrile (FMBP)

Figure 1 Molecular structure of 4′-halomethyl-2-biphenylcarbonitrile compounds along with numbering of atom.

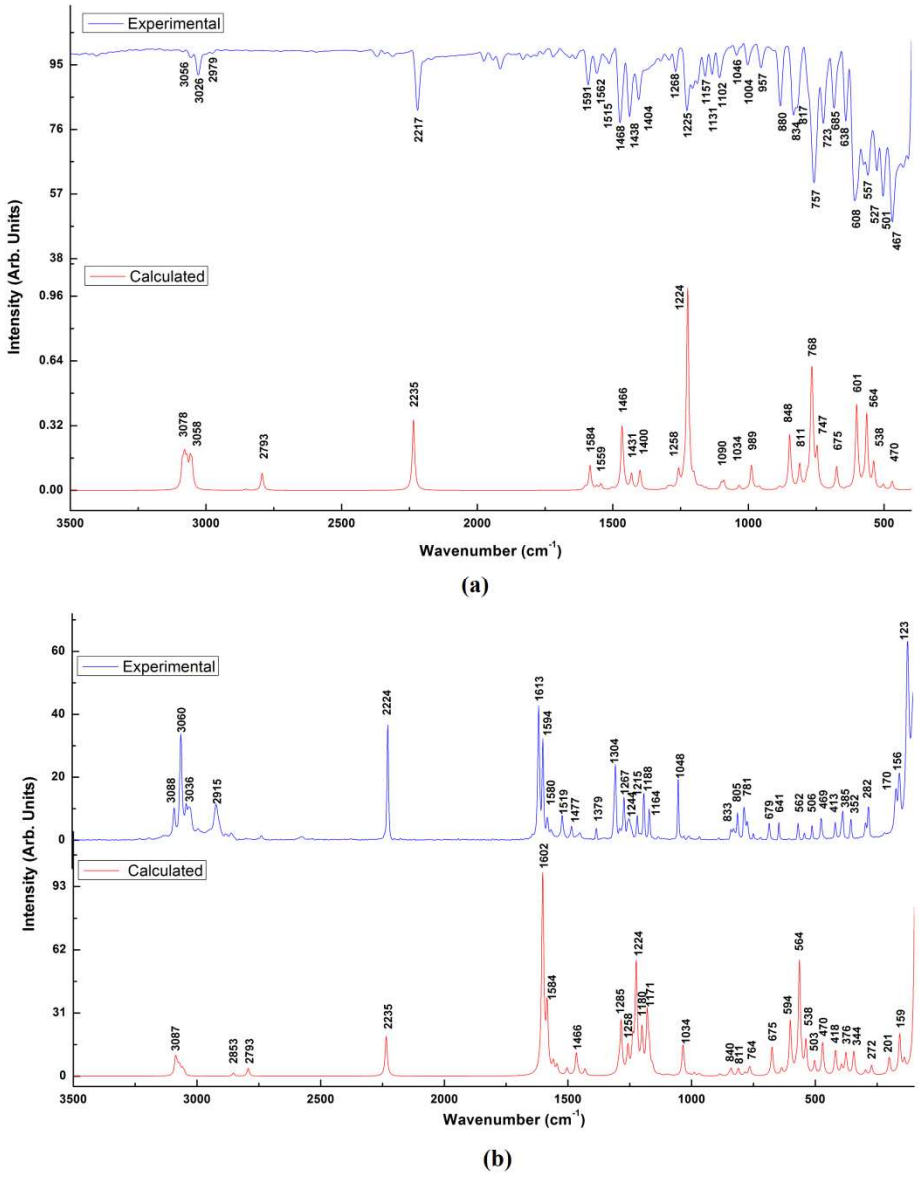

Figure 2 Experimental and simulated (a) FT-IR and (b) FT-Raman spectra of BMBP

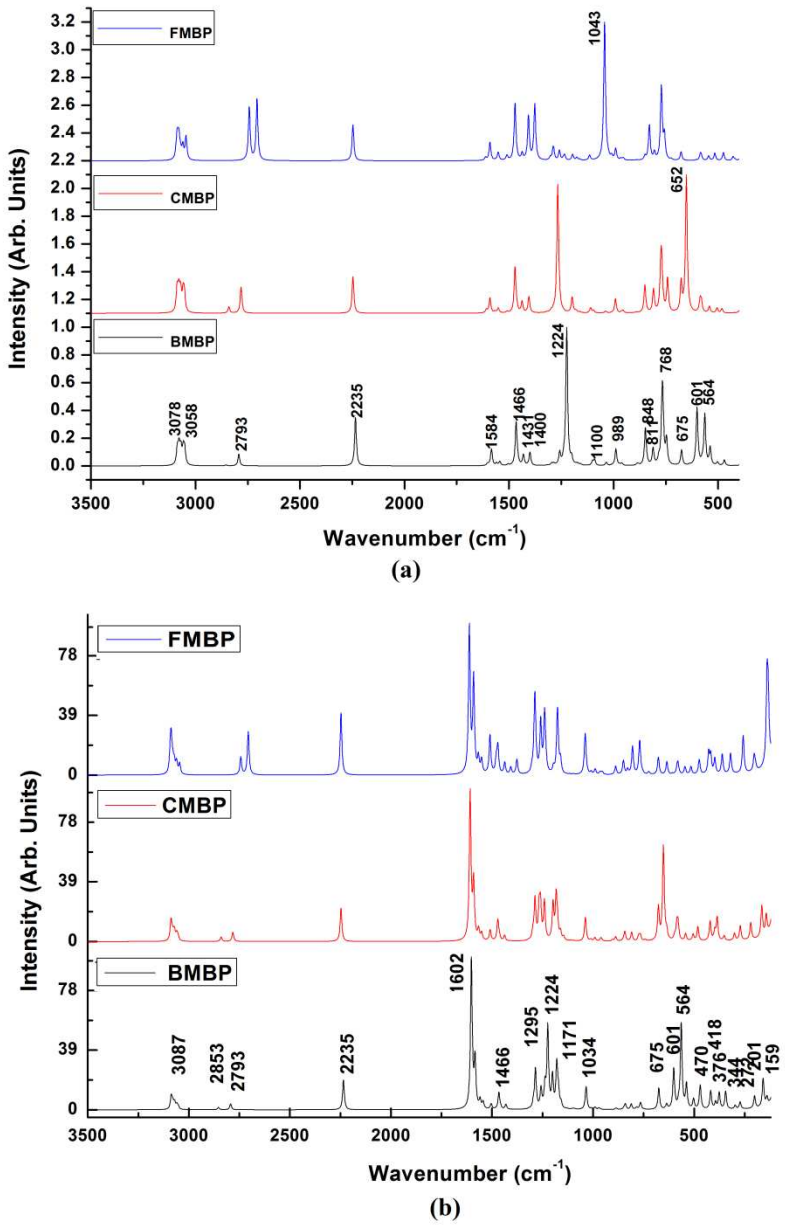

Figure 3 Simulated (a) FT-IR and (b) FT-Raman spectra of BMBP, CMBP and FMBP.

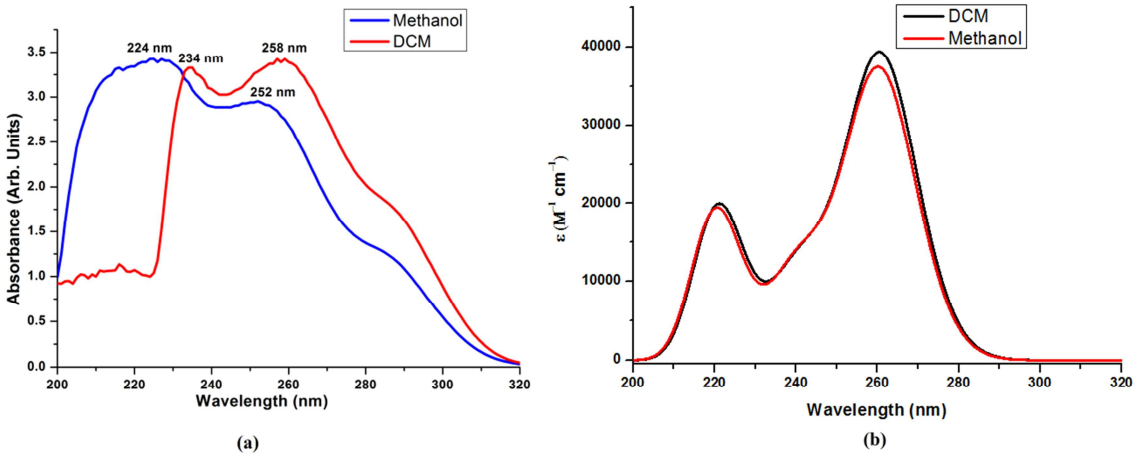

Figure 4 (a) Experimental and (b) theoretical UV-visible spectra of BMBP in dichloromethane and methanol.

Highlights

- Vibrational and electronic spectra of 4′-halomethyl-2-biphenylcarbonitrile compounds
- The nonlinear optical and thermodynamics properties of 4′-halomethyl-2-biphenylcarbonitrile
- The molecular extinction coefficient of charge transfer peak is decreasing with an increasing electronegativity of the halogen substituent.